Global Unsteady Pressure Fields Over Turrets In-Flight

Nicholas De Lucca[1], Stanislav Gordeyev[2] and Eric Jumper[3]
University of Notre Dame, Notre Dame, IN, 46545

Point pressure measurements were performed on a hemisphere-on-cylinder turret in-flight and in the Whitefield wind tunnel at the University of Notre Dame. Measurements were performed over a range of Mach numbers between 0.33 and 0.8. The pressure coefficients (c_p) was analyzed versus viewing angle for each Mach number and were compared with previous experiments and theoretical values based on the potential flow. At transonic Mach numbers, the dominant frequencies of the motion of the local shock over the turret were investigated. The turret wake was also investigated and it was shown that the "smiles" cut-outs and the local shock can have a "regularizing" effect of decreasing higher frequency fluctuations while increasing low frequency fluctuations. Unsteady forces acting on the turret were computed from the pressure fields and their dependence on the Mach number and turret geometry was discussed.

Nomenclature

Az	=	Azimuthal angle in degrees
El	=	Elevation angle in degrees
α	=	Viewing angle in degrees
β	=	Modified elevation angle in degrees
M	=	Mach Number
P	=	Turret surface pressure relative to local atmospheric pressure
$\overline{p}$	=	Mean component of turret surface pressure
p	=	Fluctuating component of turret surface pressure
p_∞	=	Freestream pressure

[1] Graduate Student, Department of Mechanical and Aerospace Engineering, Hessert Laboratory for Aerospace Research, Notre Dame, IN 46556, AIAA Student Member.
[2] Research Associate Professor, Department of Mechanical and Aerospace Engineering, Hessert Laboratory for Aerospace Research, Notre Dame, IN 46556, AIAA Associate Fellow.
[3] Professor, Department of Mechanical and Aerospace Engineering, Hessert Laboratory for Aerospace Research, Notre Dame, IN 46556, AIAA Fellow.

ρ_∞ = Freestream density

V_∞ = Freestream velocity

I. Introduction

For directed energy and free-space communication applications, the hemisphere-on-cylinder turret is a commonly used geometry to maximize the field-of-regard for a given system. But the non-optimal aero-dynamical shape creates a complex unsteady flow field around the turret, affecting aero-optical environment both directly, by changing density field over the beam aperture [1] and indirectly, by creating unsteady aero-buffeting, which results in increased mechanical vibrations of optical components inside the turret [2]. The aerodynamic environment changes at high transonic speeds, when the flow field is modified by the presence of a local unsteady shock formed on top of the turret [1].

The aero-dynamic environment around turrets has been studied extensively in recent years using a variety of techniques. Optical wavefront and jitter measurements have been performed for different turret configurations both in flight [3,4,5] and in wind tunnels [6,7,8]. Unsteady surface pressure measurements at low subsonic speeds have also been performed in a tunnel using a combination of Pressure Sensitive Paint [2,9,10] and unsteady pressure sensors, although with a very sparse array of sensors [6,9]. Along with the experimental work performed on optical turrets, extensive CFD studies have been performed to predict their aero-optical and aerodynamic performance [11, 12,13].

Surface pressure carries information about flow features that are occurring very near the surface of a body. For aero-optical applications surface information can appear to have limited usefulness, given the integrated nature of aero-optics. However, the information about surface pressure field of a turret can be indirectly used to predict aero-optical effects and improve turret design. First, surface pressure directly drives mechanical jitter in directed energy systems, through the unsteady force applied to the turret [6,9]. Knowledge of surface pressure distributions can facilitate the design of turrets that minimize induced mechanical jitter. Second, the signatures imprinted on surface pressure can be used to study the flow features that cause them. Correlations between surface pressure and optical measurements have been performed to identify specific flow features that have an aero-optical impact [6]. Also, using surface pressure as an input into a feed-forward adaptive optic system was shown to be very promising way to decrease resulted aero-optical distortions [14]. Finally, surface pressure information can be used to validate

CFD studies on turrets. By improving the ability to predict flows around a turret via computational means, the design of turrets for specific directed energy systems can be streamlined.

As mentioned above, at high transonic speeds additional shock-related effects start modifying the flow around the turret. To study the transonic flow at realistic Reynolds numbers, it requires specially-designed and expensive tunnels with porous tunnel walls to eliminate the tunnel blockage effects; so far only limited steady-state numerical studies [13,15] and preliminary experimental work over hemispheres [16,17] were performed. Recently developed AAOL-T program [18] allows to perform aero-optical measurements in flight at subsonic and transonic speeds up to M=0.85. The program, which is a successor of AAOL program, uses two Falcon 10 planes, flying in close formation and provides a unique and affordable opportunity to perform aero-optical and aero-dynamic research at realistic flight conditions.

In this paper, recent experimental measurements of unsteady pressure on the surface of a turret with realistic features, collected in flight for a range of Mach numbers between 0.5 and 0.8 and in the tunnel at M = 0.33 and M = 0.4, will be presented and discussed. The main purpose of flight tests was to study changes in unsteady pressure fields between subsonic and transonic speeds, with particular emphasis on the local shock dynamics, present over the turret at high transonic speeds.

II. Experimental Setup

Local surface pressure measurements were performed on the surface of a 12 inch diameter turret with geometry identical to the AAOL optical turret [3,4,5], see Figure 1, left. This turret has realistic features including trunnion gaps, “smiles” cut-outs and smaller secondary windows, indicated in Figure 1, left. The turret also has the capability to switch between a flat and conformal aperture. The turret was mounted on a frame that allowed for rotation to any desired azimuthal angle and featured a worm-gear system that allowed control the of elevation angle. Measurements were performed in-flight on the AAOL-T. Flight measurements were obtained at M = 0.4-0.6 at an altitude of 15,000 ft and M = 0.7 and 0.8 at 28,000 ft. In addition, the turret was recessed into the plane, so only the hemispherical portion of the conformal-window turret was exposed to the freestream. Finally, limited measurements were performed at the University of Notre Dame in the 3’x3’ Whitefield wind tunnel at M = 0.33 and M = 0.4, primarily for comparison purposes. The turning mechanism for the turret is shown in Figure 1, right. The turret can turn in the azimuthal direction via a hand crank attached to a gear. The elevation angle was adjusted by a worm gear that was fed into the turret itself.

Figure 1: The turret with the conformal window mounted on the AAOL-T, left and the interior testing bench, right.

Table 1: Tested geometry types, flight conditions and azimuthal angles

Turret Type	Altitude/Mach and Az-anlges (in degrees)
Hemisphere, Conformal Window	15 kft/0.4: Az = 0 8 20 28 44 90 134 180 15 kft/0.5: Az = 0 8 20 28 44 90 134 180 15 kft/0.6: Az = 0 8 20 28 44 85 88 90 134 180 28 kft/0.7: Az = 0 8 20 28 44 85 88 90 112 134 180 28 kft/0.8: Az = 0 8 20 28 44 85 88 90 97 112 134 180
Full Turret, Conformal-Window	15 kft/0.4: Az = 0 8 20 28 44 90 134 180 15 kft/0.5: Az = 0 8 20 28 44 90 134 180 15 kft/0.6: Az = 0 8 20 28 44 85 88 90 134 180 28 kft/0.7: Az = 0 8 20 28 44 85 88 90 112 134 180 28 kft/0.8: Az = 0 8 20 28 44 85 88 90 97 112 134 180
Full Turret, Flat-Window	15 kft/0.4: Az = 0 44 82 90 97 112 123 134 180 15 kft/0.5: Az = 0 20 44 82 90 97 112 123 134 180 15 kft/0.6: Az = 0 20 44 82 90 97 112 123 134 180 28 kft/0.7: Az = 0 20 44 82 90 97 112 123 134 180 28 kft/0.8: Az = 0 8 20 44 82 90 97 112 123 134 180

The turret was instrumented with 36 unsteady pressure sensors. The sensor locations are shown in Figure 2 for the turret with the conformal window. Sensor locations varied between the flat and conformal window; flat-window turret has the same sensor arrangement, except for 7 sensors on the flat window were arranged in a hexagonal pattern. Except for the 7 sensors on the turret aperture, the pressure sensors were approximately evenly spaced around the turret. All the sensors were a 10 psi differential Kulites. The sensors were all referenced to the turret interior pressure, which was measured independently with an absolute pressure sensor. Pressure measurements in flight were acquired for three turret geometries and 5 Mach numbers at 25 kHz for 20 seconds for a wide range of azimuthal angles, see Table 1; the zero azimuthal angle aligned with the incoming freestream flow. The elevation was fixed at 45 degrees for all flight and tunnel tests.

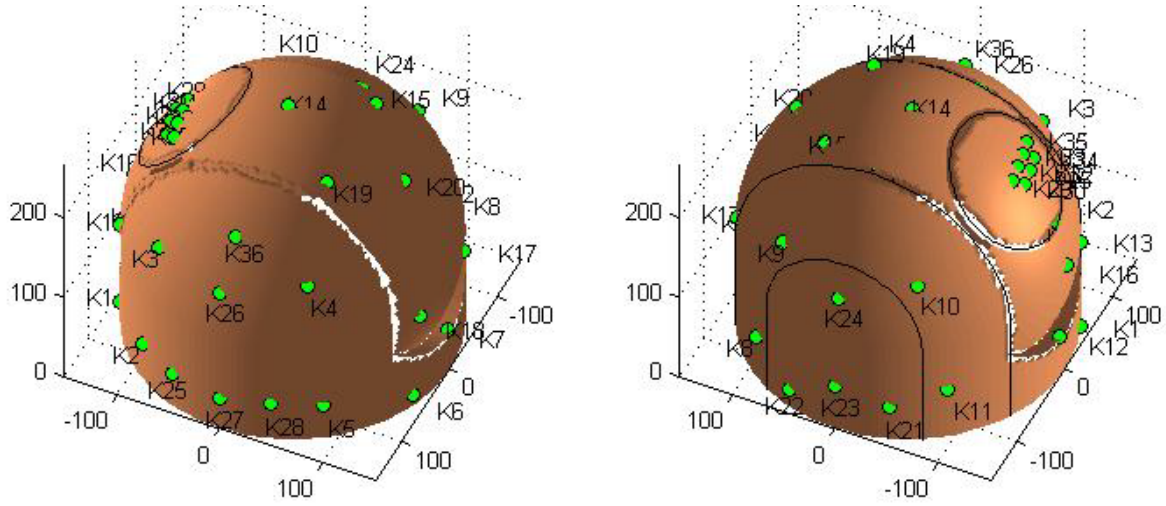

Figure 2: Locations of the 36 Kulite pressure sensors with the conformal window.

III. Data Analysis

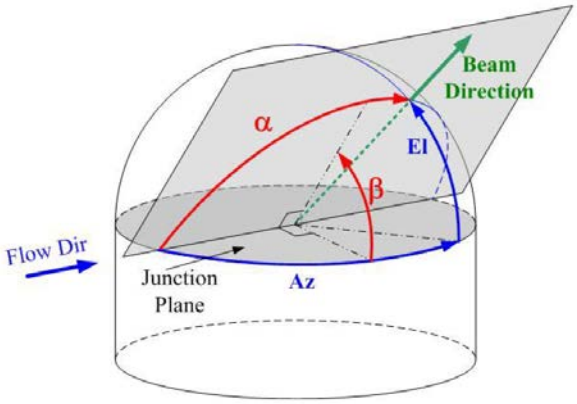

Figure 3: Relationship between azimuthal (Az) and elevation (El) angles to viewing angle (α) and modified elevation angle (β). From [4].

Pressure measurements were split into mean and unsteady components,

$$P = \bar{p} + p(t). \tag{1}$$

The mean component was used to compute the pressure coefficient for each sensor,

$$c_p = \frac{\bar{p} - p_\infty}{1/2\,\rho_\infty V_\infty^2}. \tag{2}$$

It has been previously shown that upstream of the separation, the pressure coefficient distribution around the turret nearly matches that of the potential solution for flow around a sphere [1]. To analyze the distribution of the unsteady pressure component around the turret at various Mach numbers, the RMS pressure was normalized by the dynamic pressure

$$c_{p,RMS} = \frac{p_{RMS}}{1/2\,\rho_\infty V_\infty^2}\,. \tag{3}$$

Additionally, the azimuthal (Az) and elevation (El) angles of the various sensors were recast into a coordinate system that is more useful from a fluid dynamics perspective. The viewing angle is given by

$$\alpha = \cos^{-1}\left(\cos(Az)\cos(El)\right), \tag{4}$$

and the modified elevation angle is given by

$$\beta = \tan^{-1}\left(\frac{\tan(El)}{\sin(Az)}\right). \tag{5}$$

This is shown in Figure 3.

To fully capture the mean pressure distribution on the turret, computed c_p values from three different azimuthal angles, 0°, 8° and 20° were combined and plotted versus the viewing angle, shown in Figure 4. Even though the "smiles" and trunnion gaps of the turret geometry change orientation slightly with respect to the flow direction as the turret azimuthal changes, it is assumed that for these relatively small angles, the flow around the turret is not significantly altered.

A spline-based interpolation scheme was also used to visualize and estimate global pressure field changes using only a sparse array of sensors. This interpolation method assumes that the pressure field changes smoothly between points, an assumption that can break down for transonic Mach numbers, where the shock is present on top of the turret. For cases in this regime, shock effects occur only at very specific locations on the turret. The interpolation scheme tends to spread out these short-scale effects, and by nature of using a scattered array of sensors, it is possible that a sensor would not fall in the small region that these effects occur, preventing them from appearing in the pressure field estimate entirely. Because of these two shortcomings of this pressure field estimation at transonic Mach numbers, any plots of interpolated fields at these Mach numbers are used purely for spatial visualization of pressure effects, they are not intended to be a fully accurate representation of the pressure field.

IV. Results

Subsonic Results

To provide a baseline pressure field to compare transonic data with, and to establish parity between flight data tunnel experiments that have been previously performed [1,19,20,21,22], subsonic (M = 0.4-0.5) pressure data using this turret model both in flight and in the tunnel is presented.

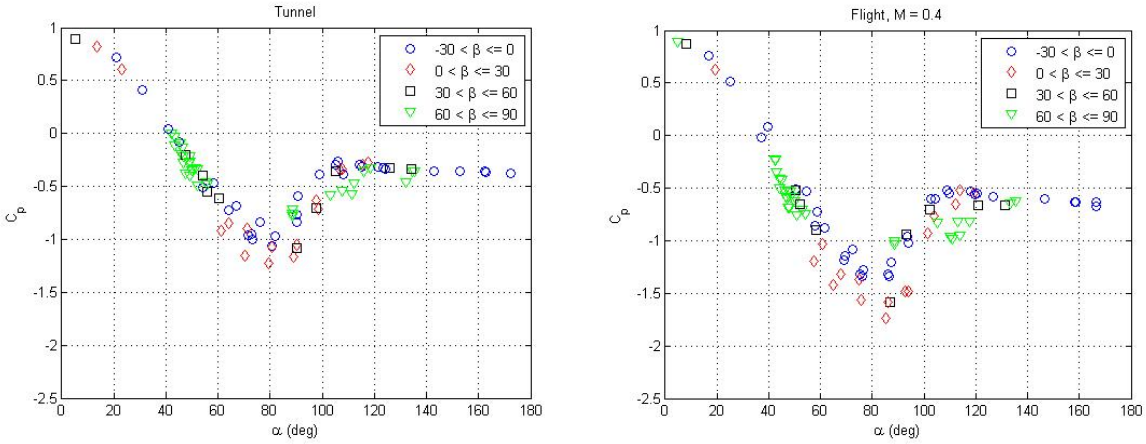

Figure 4: Pressure coefficient (c_p) versus viewing angle in the tunnel, left and in flight, right. Data broken up into bands of modified elevation angle. Both cases are at M = 0.4. "Smiles" located at Az = 0°, 180°.

Figure 4 shows the c_p versus viewing angle distribution over the turret for M = 0.4 in the tunnel, left and in flight, right. The overall shape of the c_p distributions are consistent between the flight and tunnel test and agree well with prior pressure data obtained from turrets [1,19,20,21,22]. Separation occurs when the pressure coefficient approaches a constant value. From both the tunnel and the flight data, the separation occurs at earlier $\alpha = 100°$ at lower modified elevation angles, while near the apex of the turret the separation tends to occurs at $\alpha = 115\text{-}120°$. This is consistent with prior observations as well.

The normalized RMS pressure distributions are shown in Figure 5. At $\alpha < 80°$, on the upstream portion of the turret, there are minimal pressure fluctuations. On the upstream portion of the turret, only the thin turbulent boundary layer and global pressure fluctuations are felt; these are much smaller in magnitude than those related to the separation that occurs on the downstream half of the turret. Also in this α-range there isn't any modified elevation angle dependence on the unsteady pressure component for the tunnel data. For the flight data, there is a notable increase in $c_{p,RMS}$ for $\beta < 0°$. The pressure sensors at these modified elevation angles are at the very base of the turret, and when it was mounted in flight, there was a gap between the outer shell of the aircraft and the turret, see Figure 1, left. It's possible that the increase observed in flight is due to some jetting occurring into or out of this gap.

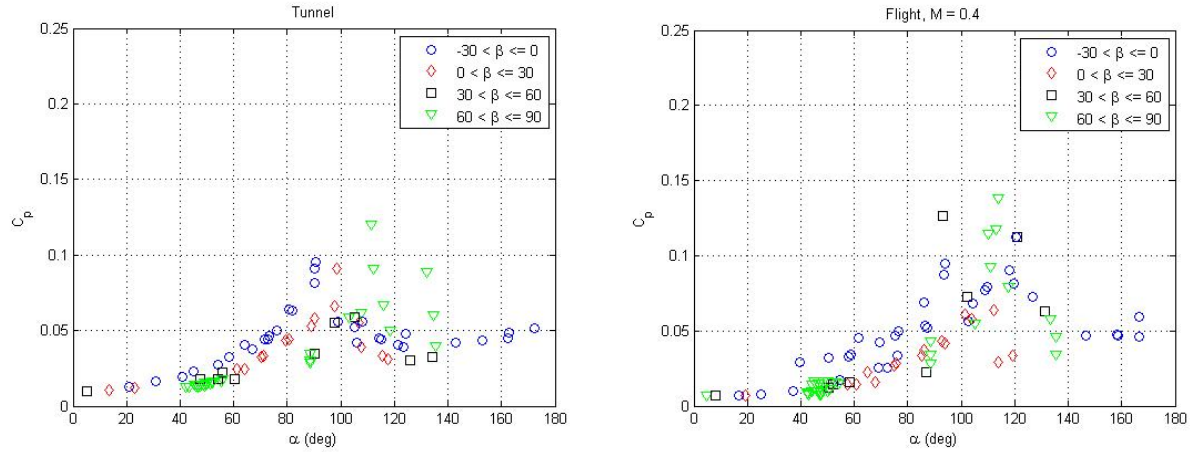

Figure 5: Normalized RMS pressure versus viewing angle in the tunnel, left and in flight, right. Data broken up into bands of modified elevation angle. Both cases are at M = 0.4. "Smiles" located at Az = 0°, 180°.

For $\alpha > 80°$, there are several distinct peaks in the RMS distribution in both the tunnel data and the flight data. These peaks are related to the location of the separation line on the turret. It has been shown that the separation is not steady [2], and as previously established, has a location that is dependent on the modified elevation angle. Each modified elevation angle band has one distinct peak at $\alpha < 120°$ and the location of the peak is consistent with the separation location observed in the steady pressure data. Near the base of the turret, separation occurs at $\alpha \approx 90°$. Moving towards the turret apex, the separation is delayed until $\alpha \approx 115°$. For $\alpha > 130°$-$140°$, the $c_{p,RMS}$ approaches a constant value of 0.05. Sensors in this region lie directly in the separated wake and experience similar pressure fluctuations.

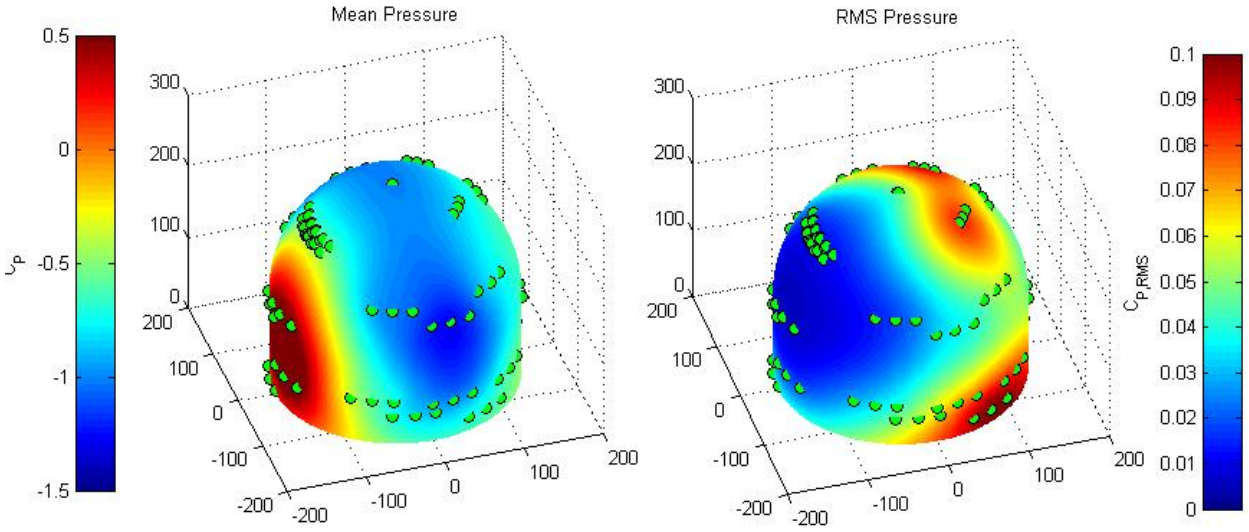

Figure 6: Interpolated mean (left) and RMS (right) pressure fields for M = 0.4 in flight Green circles indicate sensor locations. Flow goes from left to right. "Smiles" located at Az = 0°, 180°.

The mean and RMS pressures at sensor locations were also used to interpolate the global pressure field over the entire surface of the turret. This was done by computing the mean and RMS at every sensor location for the Az = 0°, 8° and 20° cases and interpolating onto a model for the turret surface. The interpolated mean and unsteady surface pressure fields for M = 0.4 in-flight are shown in Figure 6. As expected, the interpolated field data shows similar behavior to Figure 4, right and Figure 6, left. The pressure coefficient plot, Figure 6 left decreases to a minimum near α = 80-90° and goes to a constant value after separation. The RMS plot shows little pressure fluctuation upstream, except at the very base. The slight increase near the base of the turret is likely due to the necklace vortext that forms below the stagnation point. Near the apex of the turret, there is a band of increased fluctuations. This band is related to the separation line movement. The movement of the separation line has been previously studied using PSP in [2]. Near the base of the turret, on the downstream half, there is also an increase in RMS pressure. From the same PSP experiment [2], it was shown that small scale turbulent vortices shed off the turret in this region, causing the increase in RMS pressure. Though not shown, these distributions are similar between the tunnel and flight cases.

Transonic Results

The pressure coefficient distributions for M = 0.7 and 0.8 from the flight test are shown in Figure 7. For the upstream portion of the turret, $\alpha < 80°$, the distributions are nearly unchanged from the subsonic cases. In this range, the flow is accelerating and there are no transonic effects that alter the flow behavior from the subsonic regime. However, at $\alpha > 80°$, there isn't a modified elevation angle dependence on the separation line location. Separation appears to occur at the same approximate angle ($\alpha \approx 100°$) for all modified elevation angle bands. In the transonic regime, the flow separation is no longer caused by the increasing magnitude of the adverse pressure gradient as the flow decelerates at $\alpha > 90°$; instead, a shock forms on the turret and induces the separation. The lack of variance in the separation location indicates that the shock occurs at approximately the same viewing angle over the entire turret.

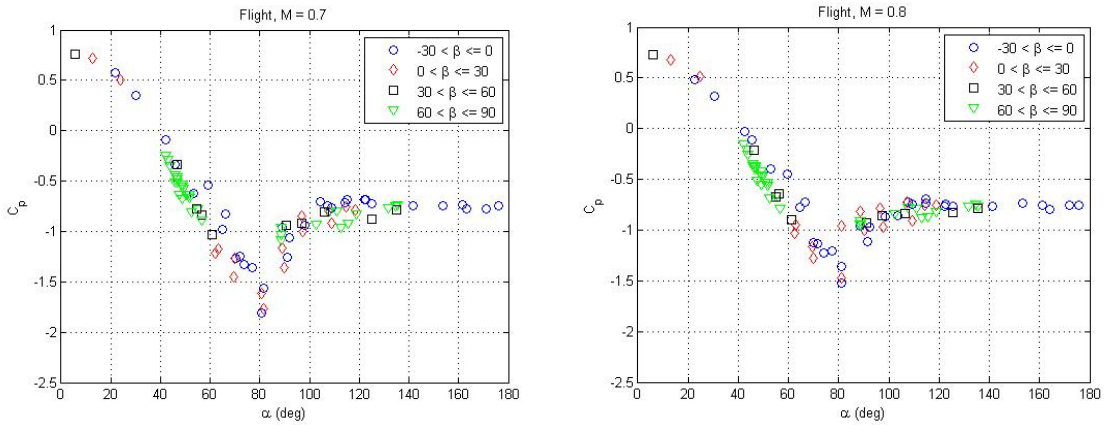

Figure 7: Pressure coefficient (c_p) versus viewing angle in the flight at M = 0.7, left and in M = 0.8, right. Data broken up into bands of modified elevation angle. "Smiles" located at Az = 0°, 180°.

For $c_{p,RMS}$ in the transonic regime, Figure 8, there are significantly different trends than observed in the subsonic case, Figure 5. Even though there is good agreement between the transonic and subsonic mean pressure distributions at $\alpha < 80°$, the unsteady pressure component varies significantly. There are substantial differences between M = 0.7 and M = 0.8 for this region. The RMS pressure remains consistent for M = 0.7 until $\alpha = 40°$, at which point there is an increase that appears to depend heavily on modified elevation angle. For M = 0.8, the RMS pressure decreases slightly until $\alpha = 80°$. There is also evidence that the magnitude of the pressure fluctuations depends on the modified elevation angle for M = 0.8 at $40° < \alpha < 80°$, as opposed to being relatively independent of it, as was seen in the subsonic cases.

For both M = 0.7 and M = 0.8, there is a sharp peak at $\alpha = 80°$-82°, which is related to the unsteady motion of the shock on the turret, observed optically in [23]. This peak location is close to the mean shock location observed in optical data presented in the companion paper [23]. As this peak location doesn't change with the modified elevation angle, it indicates the shock location occurs at the same viewing angle for all modified elevation angles. This is consistent with the mean pressure results, shown in Figure 7. The pressure fluctuations just before and just after the shock are at least partially driven by its motion. Analysis of aero-optical data [23] had revealed that the shock moves between approximately $70° < \alpha < 90°$. The fact that the shock spends the majority of its time right near $\alpha = 80°$-82° [23] causes the large peak at this location.

Just after the shock, at $90° < \alpha < 120°$, there are elevated levels of pressure fluctuations compared to the subsonic case. These fluctuations are likely driven by the shock-induced separation. Further downstream, the pressure fluctuations follow a similar trend to the subsonic case, as they remain relatively constant. There is a slight

increase in $c_{p,RMS}$ levels in the wake compared to the subsonic case, indicating relatively stronger turbulence levels. This is the evidence that the shock-induced separation increases overall turbulence levels in the wake.

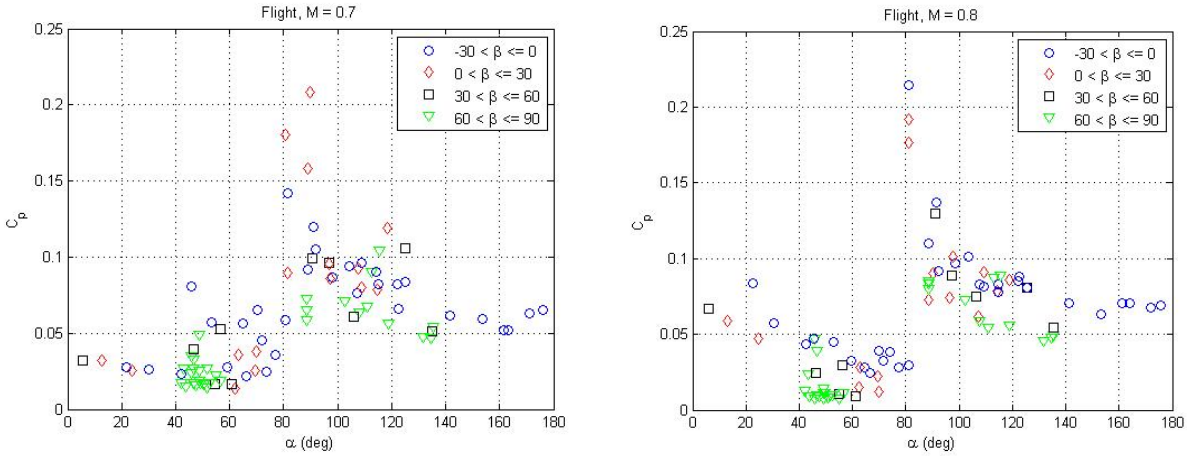

Figure 8: RMS Pressure coefficient ($c_{p,RMS}$) versus viewing angle in the flight at M = 0.7, left and in M = 0.8, right. Data broken up into bands of modified elevation angle.

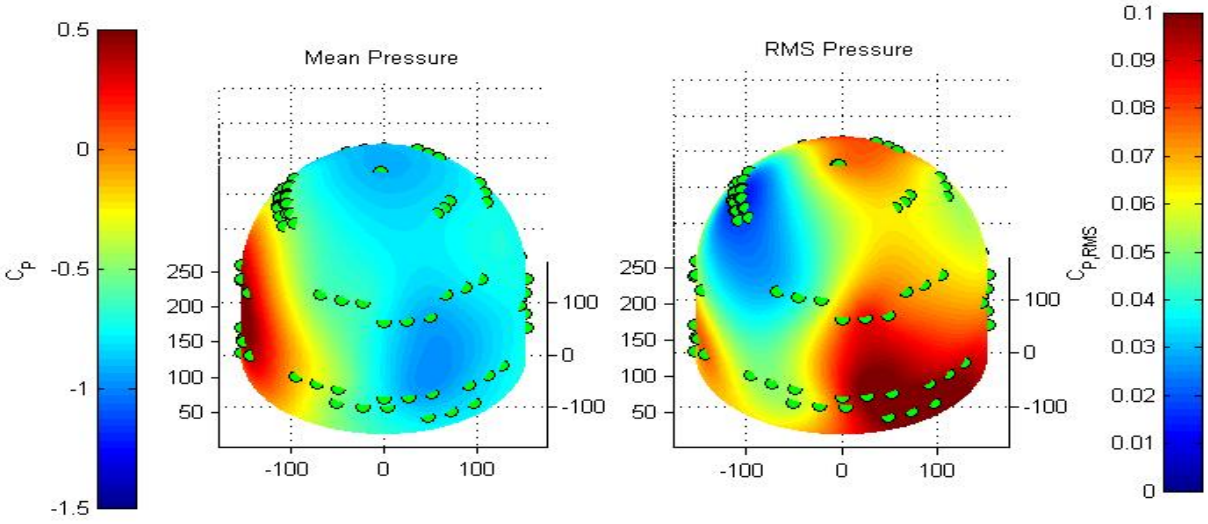

Figure 9: Interpolated mean (left) and RMS (right) pressure fields for M = 0.8 in flight. Green circles indicate sensor locations. Flow goes from left to right. “Smiles” located at Az = 0°, 180°.

The interpolated mean and RMS pressure fields for M = 0.8 are shown in Figure 9. As it was discussed before, due to the nature of the flow at transonic mach numbers, the interpolated fields from a scattered sensor array cannot accurately capture small features of the pressure fields, especially in the region near the shock, if there are not many sensors present. However, in locations where there is sufficient sensor density, it is possible to glean some field information using the interpolations. The mean pressure field is very similar to the subsonic cases. It is possible to see the approximate shock location by the sharp gradient of RMS pressure in Figure 9, right. This area corresponds to the large peak seen in Figure 8, right. Near the base of the turret, after separation occurs, there is a

region of elevated pressure fluctuations. This is likely similar to the same area in the subsonic case. Fluctuations in this region likely correspond to small scale vortices that form near the base of the turret. There is a marked increase in normalized pressure fluctuations in this region compared to the subsonic case, however. This increase is likely due to the shock-induced separation magnifying the effect of the vortices. A similar effect was seen in the purely subsonic case when the "smiles" of the turret were aligned cross-stream with the flow [2]. The increase in pressure fluctuations for both cases results from additional turbulent structures being introduced near the base of the turret. For this transonic case, vortical structures are introduced by the shock-induced separation, while for the subsonic case, the structures come from flow separation over the "smiles". The only major flow feature of the turret in this region is the necklace vortex. The increase in normalized RMS pressure relative to the subsonic cases might indicate that the presence of the shock wave on the turret might be modifying the magnitude or extent of the necklace vortex. Further experiments would be required to verify this.

Shock Effect Analysis

Analysis of the spectral behavior of the local pressure sensors gives insight into the dynamics of the shock on the turret. Figure 10 shows the normalized pressure spectra for a pressure sensor right near the edge of the shock movement at M = 0.7 and M = 0.8 in flight. For both Mach numbers, there is a distinct peak at St = 0.15. At subsonic Mach numbers, a peak in this location has been associated with the movement of the separation line of the turret [2]. From Figures 7 and 8, it was shown that for transonic Mach numbers, the separation is induced by the shock and occurs prematurely. From Figure 10 it follows that the Strouhal number associated with the movement of the separation location is the same for both subsonic and transonic flow regimes. It is also evidence that the driving mechanism for the movement of the separation line may be the same for both regimes, though further experiments would be required to confirm this. This linking of the shock and the separation over the turret has been investigated previously for a 2-D turret [24].

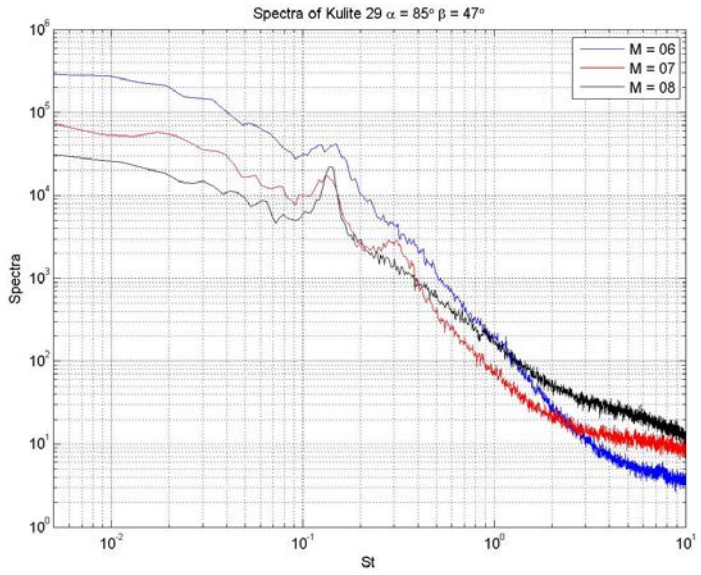

Figure 10: Pressure spectra at α = 85°, β = 47° for M = 0.8. "Smiles" located at Az = 90°, -90°.

For M = 0.7, there is also a secondary peak in the pressure signature located at St = 0.3. This second peak has not been observed for any dominant pressure modes at subsonic Mach numbers [2]. It is likely related to the fact that the shock at M = 0.7 is weaker in strength compared to M = 0.8 and not fully coupled to the separation line movement. This single peak at M = 0.8 and the double peak behavior at M = 0.7 was also observed in wavefront data in [23].

The shock at both of these Mach numbers show different characteristic frequencies than was previously observed at M = 0.65 on the AAOL [25]. At this Mach number, the shock was shown to be intermittent, with a timescale of $tU_\infty/D = 2$, which would correspond to a Strouhal number of 0.5. Because the shock at M = 0.65 is intermittent and weak, it is not forcing the separation of the turret. As it is not tied to the separation location, the shock is not forced to move at a frequency of St = 0.15 and instead moves at a higher St = 0.5. This is further evidence that the second peak at St = 0.3 for M = 0.7 is due to the shock not being fully driven by the separation. The overall frequency of the shock decreases towards St = 0.15 as Mach number increases, until the shock becomes linked to, or locked-in with the separation around the turret.

Wake Effects Analysis

The baseline subsonic wake at M = 0.6 for Az = 0, 90 and 180 is shown in Figure 11. It has been previously shown that the locations of the "smiles" can have an effect on the wake of the turret [2]. To obtain averaged wake spectra, the pressure spectra for every pressure sensor in the wake (α > 120°) were averaged together. The wake

spectra are very similar for Az = 0° and 180°; there is a weak peak at St = 0.15 and a steady decrease as St increases. The geometry of the turret for both of these angles is virtually the same, so the difference at St > 0.4 is likely due to the number and the locations of sensors in the wake to average over. Physically, there should be very little difference in the week between these two angles. At Az = 90, there is a substantial reduction in wake energy at St > 0.4. This reduction is coupled with a marked increase between St = 0.1 and St = 0.15. It was shown that aligning the "smiles" with the cross-stream direction amplifies the peak at St = 0.15, which is associated with the movement of the separation line [2]. The increased separation line movement likely has an effect of regularizing the wake, making it more periodic. The regularization increases energy at lower frequencies while pulling energy out of the higher frequencies.

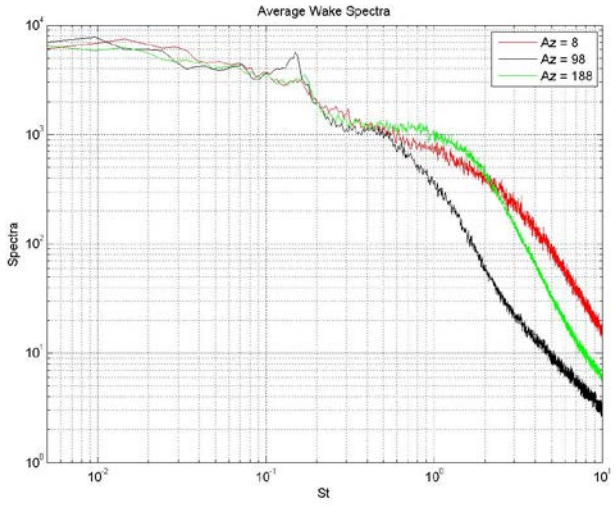

Figure 11: Average wake spectra for M = 0.6 at various Az angles.

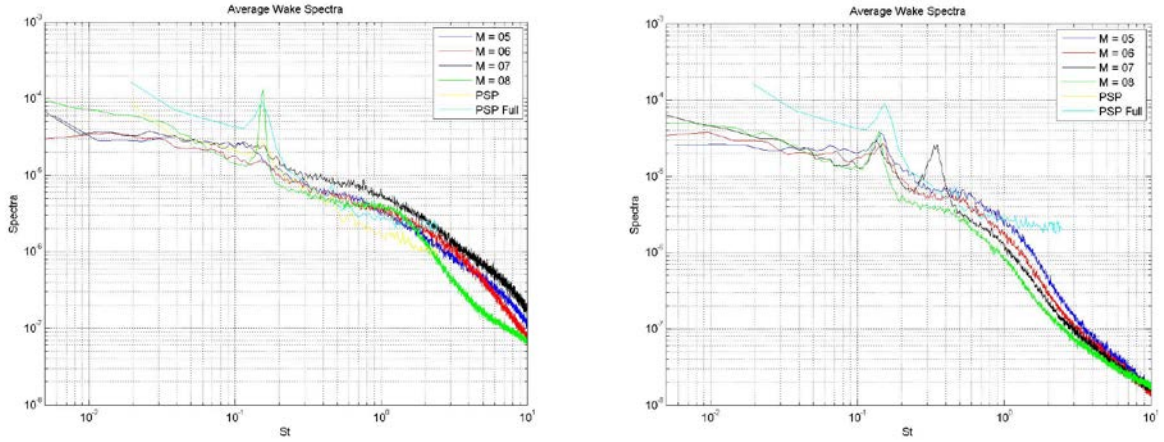

Figure 12: Normalized average wake pressure spectra for "smiles" located at Az = 0°, 180°, left, and "smiles" located at Az = 90°, -90°, right.

With the baseline established, the effect of the Mach number on wake spectra for two different "smile" locations is shown in Figure 12. For comparison sake, extracted wake spectra from the PSP experiment featured in [2] is included. As shown in Figure 8, the wake was also modified by the presence of a shock, for both M = 0.7 and M = 0.8, as there are slightly increased normalized pressure fluctuations compared to the subsonic cases in Figure 5. For M = 0.7, with the "smiles" aligned with the flow, Figure 12, left, there is an increase in pressure fluctuations across virtually all Strouhal numbers compared to the subsonic cases. The lack of any distinctive peaks for $M \leq 0.7$ indicates that the shock movement isn't being "felt" in the wake. The broadband increase in normalized pressure fluctuations relative to the subsonic cases indicates that there is more energy in the wake. It's possible that the shock is not strong enough to have a regularizing effect on the wake, and the shock-induced premature separation is simply increasing the total energy in the wake. But the shock effects is clearly present for M = 0.8, as it locks-in to and significantly amplifies the separation frequency peak at St =0.15, altimately affecting the wake dynamics.

Figure 12, right, shows the wake spectra when the "smiles" are aligned in the cross-stream direction. For M = 0.7, there are two distinct peaks in the pressure spectra, one at St = 0.15 and another at St = 3.5. The St = 0.15 peak is again related to the movement of the shock and separation line. In this case, the normalized magnitude at this peak is slightly increased over the subsonic cases. There are also reduced pressure fluctuations at St > 0.5 compared to the subsonic cases. As was previously shown in Figure 11, aligning the "smiles" in the cross-stream direction has an effect of regularlizing the wake of the turret, increasing pressure fluctuations at St = 0.15 while decreasing them for St > 0.4. It should be noted that for 0.5 < St < 10, there is a monotonic decrease in in pressure fluctuations as Mach number increases. For the M = 0.7 case, there is a secondary peak at St = 0.35 that is possibly due to the shock motion which is not related to the St = 0.15 separation line movement. Further experiments would be required to investigate this peak.

For M = 0.8 with the "smiles" aligned with the flow, Figure 12, left, the spectra show a distinct peak at St = 0.15 and reduced pressure fluctuations at St > 0.15 compared to the subsonic cases. This behavior is consistent with the regularization of the wake that has been previously discussed. The shock appears to pull energy out of St > 0.15 frequencies and greatly increase energy at St = 0.15. As this behavior is not present at M = 0.7, it is likely that the shock must be strong enough to fully couple with the separation region before the wake begins to regularize. With the "smiles" aligned in the cross-stream direction, there is still the characteristic peak at St = 0.15 with the reduction in energy at St > 0.15 compared to the subsonic cases. Similar to M = 0.7, the St = 0.15 peak has a slightly higher

magnitude compared to the subsonic cases. This observation suggests that the shock might have an effect on the regularization of the wake, but the "smiles" are the major driving feature when they are aligned with the cross-stream direction. This is definitely an area where further experiments with a "smile"-covered turret are needed.

Unsteady Force Analysis

The interpolated pressure fields around the turret were integrated to compute the unsteady forces acting on the turret. As they are computed from interpolated pressure fields from scattered data, they are subject to the same reservation as detailed above: small spatial features with length scales smaller than the pressure sensor spacing may not be properly resolved. For this reason, the exact values of the unsteady force are only an estimate; however, potential trends regarding Mach number and the window azimuth angle can be determined. The computed forces are normalized by the dynamic pressure and the cross-sectional area of the turret. The streamwise and cross-stream direction RMS forces are shown in Figure 13, left and right respectively.

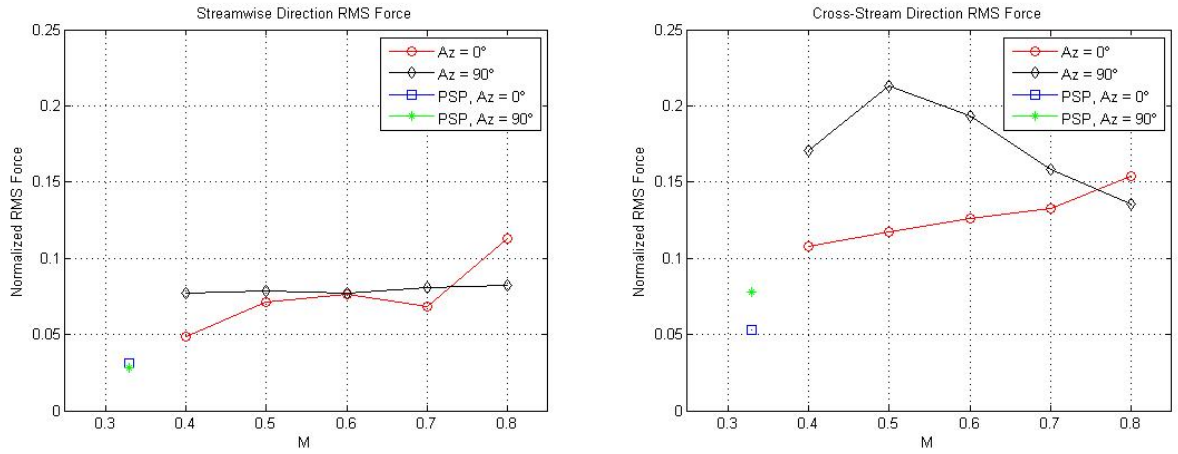

Figure 13: The RMS forces in the streamwise (left) and cross-stream (right) directions at Az = 0° and 90° versus Mach number.

In the streamwise direction, there is little change in RMS forcing between the M = 0.4 to M = 0.7 cases at Az = 0°. There is, however a large increase at M = 0.8. This is likely due to the stronger, periodic shock and additional turbulent structures near the base of the turret at M = 0.8 compared to the previous two cases, as shown in Figure 9. At Az = 90°, however, there is little change between Mach numbers. It's possible that the presence of the "smiles" aligned in the cross-stream direction modifies the shock dynamics such that it has a lesser effect on the unsteady forcing of the turret. These normalized RMS force values are larger than were observed in [9], by approximately a factor of 2-2,5, for various reasons. First, the upstream half of the turret was not resolved in [9], which means that force contributions from pressure fluctuations on the front half of the turret were not included in

the integrated force values. Integrating force contributions over only half of the area will reduce the total RMS forcing. Second, the total RMS forces reported in [9] were for M = 0.33 in the wind tunnel, which is a different flow regime than in flight at M = 0.6-0.8. Finally, just as the interpolation scheme used in this paper may not capture small scale pressure fluctuations if they do not occur over the sensors, any small scale effects that are captured by the sensors can be interpolated to occur over a large spatial scale than is physical, artificially amplifying their force contribution. In terms of real force values RMS forces in the streamwise direction are near 25-30 N, up to 41N for M = 0.8 at Az = 0°.

For the cross-stream direction forcing, Figure 13, right, there is a marked increase compared to the streamwise direction forcing at both azimuthal angles and Mach numbers. This is similar to what has been observed in flight in [9]. For the Az = 0° case, there is little difference between M = 0.6 and M = 0.7, with a marked increase at M = 0.8. This again is likely due to the stronger and more periodic shock. For Az = 90°, however, the largest normalized unsteady forcing occurs at M = 0.5, with a monotonic decrease going to M = 0.8. This is evidence that not only the "smiles" might interfere with the shock's effect on the unsteady forcing, the converse is also true for the cross-stream forces. The shock appears to mitigate some of the forcing increase due to the "smiles", with a larger effect as shock strength increases. Similar to the streamwise direction unsteady forcing, there is a slight increase at M = 0.7 going from Az = 0° to Az = 90° and a decrease at M = 0.8 for the same azimuthal angle change. The non-normalized RMS force values in the cross-stream direction are between 35 and 70 N.

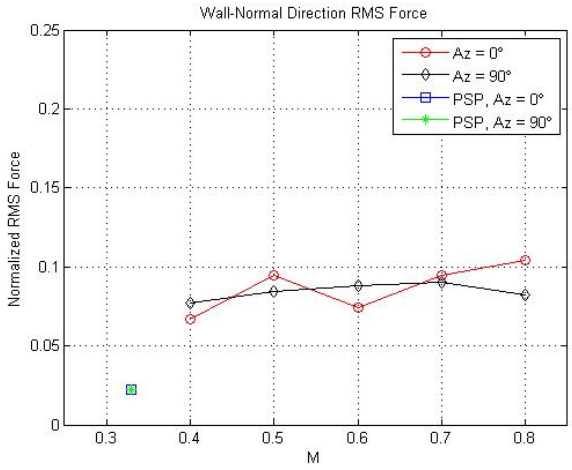

Figure 14: The wall-normal direction RMS forcing at Az = 0° and 90° versus Mach number.

The wall-normal direction forcing is shown in Figure 14. Again, similar to what was observed in [9], the wall-normal forcing is less than the cross-stream direction forcing for all cases. There is little difference between the

two azimuthal angles across all Mach numbers. The largest wall-normal forcing occurs at Az = 0°, M = 0.7-0.8, when the shock is present on the turret. For Az = 90° at both M = 0.7 and M = 0.8, there is a very slight decrease compared to the Az = 0° cases. Again, this is evidence that the "smiles" lessen the effect of the shock on the unsteady forcing of the turret. Further experiments are required to investigate these trends. Non-normalized RMS force values in the wall-normal direction are very similar in value to the streamwise forcing.

Force Spectral Analysis

The streamwise direction force spectra are shown in Figure 15. At Az = 0°, Figure 15 left, there is little variation in the pressure spectra from M = 0.5 to M = 0.8. The only substantial variation occurs at St < 0.1 for M = 0.8, there is a marked increase compared to the other Mach numbers. It's possible this low frequency increase is related to the shock, but additional testing would be required to confirm. There isn't much difference between M = 0.5 and M = 0.6 at Az = 90°, Figure 15 right, as well. There is a single peak at St = 0.6 for M = 0.5 that is not present at the other Mach numbers, but its origin is unclear from the pressure data alone. The spectra for M = 0.7 and M = 0.8 are also very similar; there is a characteristic peak between St = 0.3 and St = 0.4 at M = 0.7. This is the peak associated with unsteady, non-periodic motion of the shock at M = 0.7. Its presence in the streamwise spectra indicate that the pressure signature of this non-periodic behavior is non-symmetric in the streamwise direction, which indicates that it is possibly not tied to the movement of the separation line, a feature that is primarily cross-stream antisymmetric [2,9].

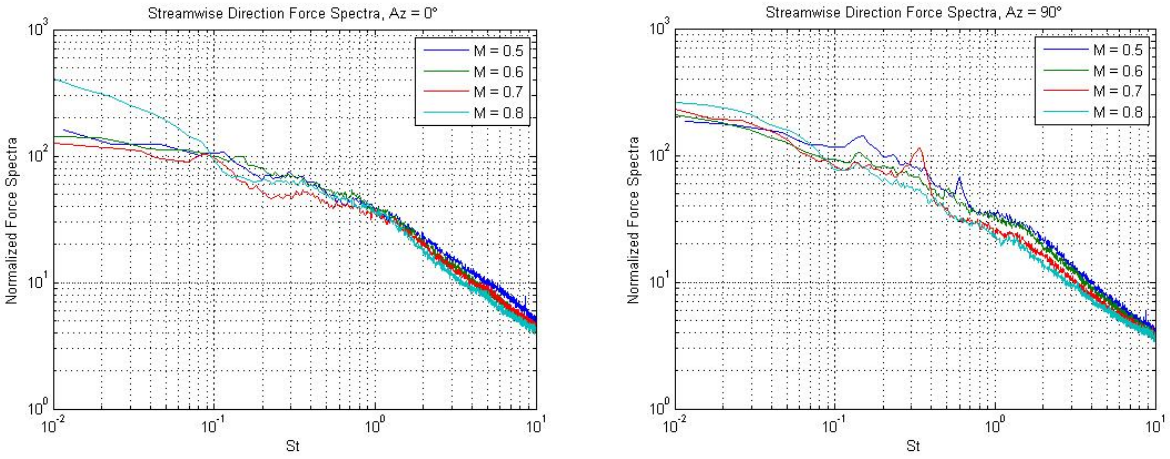

Figure 15: Streamwise direction force spectra at Az = 0°, left, and Az = 90°, right.

Cross-steam direction force spectra are shown in Figure 16. There is little variation between the two subsonic, M = 0.5 and M = 0.6 cases at Az = 0°. For M = 0.7, there is a broadband increase compared to the other three cases between St = 0.2 and St = 1. This broad band increase is potentially due to the non-periodic unsteadiness

in the shock that was both in the wake spectra in Figure 12 and in the wavefront spectra from [23]. For the M = 0.8 case, there is a very strong peak at St = 0.15, just as observed in the wake spectra previously. The shock in this case is coupled to the separation line movement and amplifying its effect; the separation line movement was also shown to have an antisymmetric character in the cross-stream direction in [2]. These two facts indicate that there should be a strong peak at St = 0.15 in the M = 0.8 data, which was observed. At Az = 90°, Figure 16 right, the cross-stream force spectra follow very similar trends to the Az = 90° wake spectra from Figure 12 right. All four Mach numbers exhibit a similar strength peak at St = 0.15. The separation line movement, which is responsible for this peak, is dictated by the "smiles" at this viewing angle, so the peak strength is expected to be Mach number invariant. There is consistent reduction at St < 0.15 and St > 0.5 as the Mach number increases. There is also a fall off that starts at 0.3 < St < 0.4 for the M = 0.7 case, as has been observed in both the wake spectra and the wavefront spectra [23].

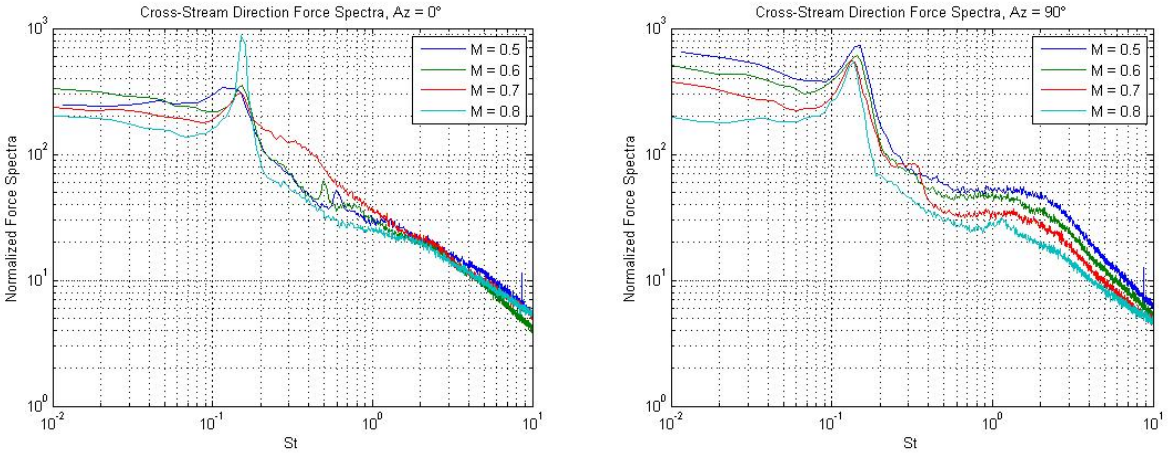

Figure 16: Cross-stream direction force spectra at Az = 0°, left, and Az = 90°, right.

The wall-normal direction force spectra are shown in Figure 17. At Az = 0°, left, there is smaller variation between the Mach numbers compared to the cross-stream forcing. Similar trends to what was observed in the wake spectra and streamwise direction forcing are found, though. M = 0.5 and M = 0.6 are very similar, though there is an increase in high frequency (St > 0.4) content at just M = 0.5. The source of this difference is not readily apparent from the pressure data alone. There is a broadband increase at M = 0.7 again, from St = 0.1 to St = 1. The M = 0.8 forcing is also similar, with a distinct peak at St = 0.15 and an increase compared to the other Mach numbers at St < 0.1. As detailed previously, the changes at M = 0.7 and M = 0.8 are due to the character of the shock at those Mach numbers. For Az = 90°, Figure 17 right, the shock is not the dominating feature on the turret for the forcing, as there is minimal difference across all the studied Mach numbers. This is consistent with the wake spectra at this viewing angle; the "smile" effect dominates the wall-normal forcing.

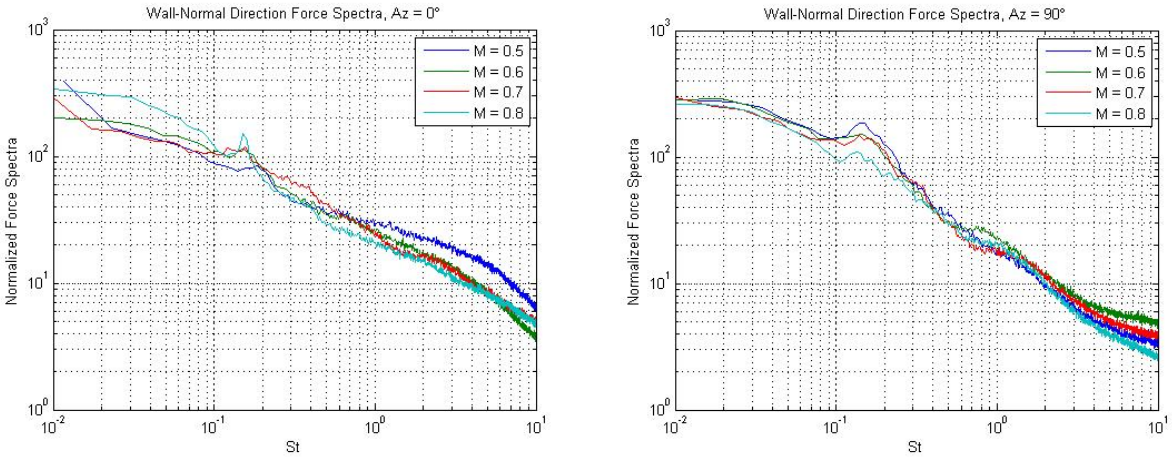

Figure 17: Wall-normal direction force spectra at Az = 0°, left, and Az = 90°, right.

V. Summary

Point pressure measurements were performed in-flight on the AAOL and in the Whitefield wind tunnel at the University of Notre Dame. Flight measurements were performed at M = 0.4 – M = 0.8 at altitudes from 15 kft to 28 kft. Tunnel measurements were performed at M = 0.33 and M = 0.4. Data were acquired at various azimuthal and elevation angles with both flat and conformal windows. Pressure measurements were obtained at 36 locations using differential pressure sensors.

The pressure coefficient and RMS pressure coefficient were computed for various in-flight and tunnel cases and plotted for different viewing angles and modified elevation angles. The tunnel and flight data agreed well at subsonic ($M \leq 0.5$) Mach numbers. The primary difference between the pressure distributions in the tunnel and in flight was due to turret mounting differences. In flight, a gap existed between the turret and the aircraft shell, which could have allowed some jetting to affect pressure sensors near the turret base. For M = 0.7 and M = 0.8, the pressure coefficient was shown to be similar to subsonic cases at $\alpha < 80°$, upstream of the shock. The shock was shown to induce a premature separation and increase pressure fluctuations due to turbulent structures near the turret base. The presence of the shock was also shown to increase pressure fluctuations in the wake.

Pressure spectra were computed for a pressure sensor that was right near the shock to investigate the frequencies associated with shock movement. At both M = 0.7 and M = 0.8, there was a characteristic peak at St = 0.15 that is associated with the separation line of the turret. This peak indicates that the shock is at least partially coupled to the location of separation on the turret. At M = 0.7 there was an additional peak at St = 0.3. This additional peak is likely due to the shock being weaker and not fully coupled to the separation movement. The coupling with the turret separation was previously shown for a 2D turret in [24]. The double peak behavior at M =

0.7 and single peak behavior at M = 0.8 were observed in a companion paper that looked into wavefront measurements at these Mach numbers [23].

The pressure fluctuations in the turret wake were also investigated. It was shown that the “smiles” of the turret impact the spectral content of the pressure fluctuations in the wake. For the subsonic regime, when the “smiles” are aligned in a cross-stream direction, they have an effect of “regularizing” the wake, pulling energy out of St > 0.4 and putting it back into a peak at St = 0.15. The same effect is observed in the transonic regime at M = 0.7 and M = 0.8. The presence of a shock does appear to have an effect on the wake “regularization” at M =0.8. At M = 0.7, there was an additional peak in the wake spectra at St = 0.35 that is possibly due to shock movement. With the “smiles” aligned with the flow, there was a broadband increase in pressure fluctuations for M = 0.7. At M = 0.8, the shock alone appears to have a “regularizing” effect on the wake, decreasing pressure fluctuations for St > 0.15 and increasing them at St = 0.15.

The unsteady forcing applied to the turret was presented versus Mach number at Az = 0° and Az = 90°. The shock was shown to increase unsteady forcing applied to the turret, especially in the cross-stream and wall-normal directions at M = 0.8 and Az = 0°. However, at Az = 90°, with the “smiles” aligned in the cross-stream direction, the effect of the shock was lessened. Conversely, at M = 0.7 and 0.8, the shock was shown to reduce the effect of the “smiles” on the cross-stream direction unsteady forcing. As the forces were integrated from interpolated sparse data and not all length scales may be properly resolved, additional experiments might be required to confirm the interaction of the shock and the “smiles” and its effect on the force applied to the turret.

Force spectra were also investigated. The spectra followed similar behavior to the wake spectra. At Az = 0°, the effect of the shock could be observed in all 3 force components, though most weakly in the streamwise direction. The difference was most pronounced in the cross-stream direction, as the shock couples with the unsteady separation line movement which has an antisymmetric character in the cross-stream direction. The wall-normal direction was very similar to what was observed in the wake, and similar to the streamwise direction forcing, the differences were small compared to the differences observed in the cross-stream direction forcing. At Az = 90°, the shock-specific behavior only appears in the streamwise direction forcing, where the St = 0.3-0.4 peak at M = 0.7 appears. This peak is much lessened in the cross-stream direction forcing. Other than that peak, there is limited difference between the forcing at the various Mach numbers as the flow around the turret is dominated by a geometric feature of the turret, the “smiles”, and not by a Mach number dependent flow feature such as the shock.

Further work can be performed to confirm some of the observations and proposed mechanisms about the shock effects over the turret. The exact interaction of the shock with the “smiles” and the effect on the wake could be investigated by performing pressure measurements on a turret without “smile” features. It was shown that the freestream Mach number has an impact on the wake regularization that appears independent of the presence of the shock and the turret, and measurements at higher Mach numbers could show if this trend continues as the shock strength increases. Finally, an investigation using pressure sensors closely clustered around the shock location could give further insight into its full range of motion and correlations between the shock and the wake could be investigated to confirm its regularizing effect.

References

[1] S. Gordeyev and E. Jumper, “Fluid Dynamics and Aero-Optics of Turrets", *Progress in Aerospace Sciences*, **46**, (2010), pp. 388-400.

[2] S. Gordeyev, N. De Lucca, E. Jumper, K. Hird, T.J. Juliano, J.W. Gregory, J. Thordahl and D.J. Wittich, “Comparison of Unsteady Pressure Fields on Turrets with Different Surface Features using Pressure Sensitive Paint ”, *Experiments in Fluids*, 55, p. 1661, 2014.

[3] E.J. Jumper, M. Zenk, S. Gordeyev, D. Cavalieri and M.R. Whiteley, "Airborne Aero-Optics Laboratory”, *Journal of Optical Engineering*, 52(7), 071408, 2013.

[4] C. Porter, S. Gordeyev, M. Zenk and E. Jumper, "Flight Measurements of the Aero-Optical Environment around a Flat-Windowed Turret”, *AIAA Journal*, Vol. 51, No. 6, pp. 1394-1403, 2013.

[5] N. De Lucca, S. Gordeyev and E.J. Jumper, "In-flight aero-optics of turrets”, *Journal of Optical Engineering*, 52(7), 071405, 2013.

[6] N. De Lucca, S. Gordeyev and E. Jumper, “Effect of Surface Unsteady Pressure Field on Global Beam Jitter for a Hemisphere-on-Cylinder Turret ”, AIAA Paper 2014-0322, 2014.

[7] N. De Lucca, S. Gordeyev, E. Jumper and D.J.Wittich, “Aero-Optical Environment around Turrets at Forward-Viewing Angles ”, AIAA Paper 2013-0721, 2013.

[8] B. Vukasinovic, A. Glezer, S. Gordeyev, E. Jumper and V. Kibens, "Fluidic Control of a Turret Wake: Aerodynamic and Aero-Optical Effects", *AIAA J.*, **48**(8), pp. 1686-1699, 2010.

[9] N. De Lucca, S. Gordeyev, E. Jumper, K. Hird, T.J. Juliano, J.W. Gregory, J. Thordahl and D.J. Wittich, “ The Estimation of the Unsteady Aerodynamic Force Applied to a Turret in Flight ”, AIAA Paper 2013-3136, 2013.

[10] J.W. Gregory, H. Sakaue, T. Liu and J.P. Sullivan, ”Fast Pressure-Sensitive Paint for Flow and Acoustic Diagnostics,” *Annu. Rev. Fluid Mech.* 2014. **46**:303–30.

[11] M. Wang, A. Mani and S. Gordeyev, "Physics and Computation of Aero-Optics", *Annual Review of Fluid Mechanics*, Vol. **44**, pp. 299-321, 2012.

[12] P.E. Morgan and M.R. Visbal., "Hybrid Reynolds-Averaged Navier-Stokes/Large-Eddy Simulation Investigating Control of Flow over a Turret", *Journal of Aircraft*, **49**(*6*), pp. 1700-1717, 2012.

[13] R. Jelic, S. Sherer and R.Greendyke, "Simulation of Various Turret Configurations at Subsonic and Transonic Flight Conditions Using OVERFLOW", AIAA Paper 2012-464, 2012.

[14] R. Burns, S. Gordeyev, E. Jumper, S. Gogineni, M. Paul and D.J. Wittich, " Estimation of Aero-Optical Wavefronts Using Optical and Non-Optical Measurements ", AIAA Paper 2014-0319, 2014.

[15] W. J. Coirier, M. Whiteley, D. Goorskey, R. Drye, J. Barber, J. Stutts, C. Porter, "Aero-Optical Evaluation of Notional Turrets in Subsonic, Transonic and Supersonic Regimes", AIAA Paper 2014-2355, 2014.

[16] Fang S, Disotell KJ, Long SR, Gregory JW, Semmelmayer FC, Guyton RW. Application of Fast-Responding Pressure-Sensitive Paint to a Hemispherical Dome in Unsteady Transonic Flow. *Experiments in Fluids* **50**(6):1495-1505, 2011.

[17] Fang S, Long SR, Disotell KJ, Gregory JW, Semmelmayer FC, Guyton RW," Comparison of Unsteady Pressure-Sensitive Paint Measurement Techniques," *AIAA J.* **50**(1):109-122, 2012.

[18] Jumper, E.J., Gordeyev, S., Cavalieri, D. and Rollins, P."Airborne Aero-Optics Laboratory - Transonic (AAOL-T)," AIAA Paper 2015-0675, 2015.

[19] Achenbach E. "Experiments on the flow past spheres at very high Reynolds numbers." *J. Fluid Mech*, **54**(3), pp. 565–75, 1972

[20] Vukasinovic B, Glezer A, Gordeyev S, Jumper E, Kibens V. "Fluidic control of a turret wake, part I: aerodynamic effects," AIAA Paper 2009-0816, 2009.

[21] Nahrstedt D, Hsia Y-C, Jumper E, Gordeyev S, Ceniceros J, Weaver L, DeSandre L, McLaughlin T. "Windtunnel validation of computational fluid dynamics- based aero-optics model." *Proc. I. MechE PartG: J. AerospEng* 2009; **223**(G4): 393–406.

[22] Gordeyev S, Post M, MacLaughlin T, Ceniceros J, Jumper E. "Aero-optical environment around a conformal-window turret." AIAA J 2007, **45**(7): 1514–24.

[23] J. Morrida, S. Gordeyev, N. De Lucca, E. Jumper, "Aero-Optical Investigation of Transonic Flow Features And Shock Dynamics on Hemisphere-On-Cylinder Turrets", AIAA Paper 2015-0676, 2015.

[24] A. Vorobiev, S. Gordeyev, E. Jumper, S.Gogineni, A. Marruffo and D.J. Wittich, " Low-Dimensional Dynamics and Modeling of Shock-Separation Interaction over Turrets at Transonic Speeds ", AIAA Paper 2014-2357.

[25] N. De Lucca, S. Gordeyev and E.J. Jumper, "In-flight aero-optics of turrets", *Journal of Optical Engineering*, 52(7), 071405, 2013.